

An experimental and theoretical study into the valence electronic structure of bicyclo[2.2.1]hepta-2,5-dione

This article has been downloaded from IOPscience. Please scroll down to see the full text article.

2006 J. Phys. B: At. Mol. Opt. Phys. 39 2411

(<http://iopscience.iop.org/0953-4075/39/11/008>)

View [the table of contents for this issue](#), or go to the [journal homepage](#) for more

Download details:

IP Address: 136.186.7.66

The article was downloaded on 04/05/2010 at 05:51

Please note that [terms and conditions apply](#).

An experimental and theoretical study into the valence electronic structure of bicyclo[2.2.1]hepta-2,5-dione

D B Jones¹, M A Bolorizadeh^{1,6}, M J Brunger¹, S Saha², F Wang²,
R Gleiter³, J Bueber³ and D A Winkler^{4,5}

¹ School of Chemistry, Physics and Earth Sciences, Flinders University, GPO Box 2100, Adelaide SA 5001, Australia

² Centre for Molecular Simulation and Faculty of Information and Communication Technologies, Swinburne University of Technology, PO Box 218, Hawthorn, Victoria 3122, Australia

³ Organic Chemistry Institute, University of Heidelberg, Im Neuenheimer Feld 270, D-69120, Germany

⁴ CSIRO Molecular Science, Private Bag 10, Clayton South MDC, Victoria 3169, Australia

⁵ School of Chemistry, Monash University, PO Box 23, Victoria 3800, Australia

E-mail: michael.brunger@flinders.edu.au

Received 3 February 2006

Published 8 May 2006

Online at stacks.iop.org/JPhysB/39/2411

Abstract

The results from an electron momentum spectroscopy (EMS) study of the outer valence electronic region of bicyclo[2.2.1]hepta-2,5-dione ($C_7H_8O_2$) are reported for the first time. The measured binding energy spectra are presented for the azimuthal angles 0° , 10° and $0^\circ + 10^\circ$, respectively, and are compared to new He(I) photoelectron spectroscopy results, which are measured as a part of this work. These experimental data are compared further with results from theoretical computations, using various methods including Hartree–Fock, density functional and an outer valence Green’s function theory. Measured orbital momentum distributions are compared on an orbital by orbital basis against those obtained by calculations which employ the plane-wave impulse approximation. These calculations use orbital wavefunctions obtained from Hartree–Fock and density functional theory with a couple of generalized gradient approximation exchange correlation (XC) functionals and the DGauss triple zeta valence polarization basis set. Agreement between the measured and calculated momentum distributions was found to be only fair. Nonetheless, the orbital momentum distributions of the molecule still provide an orbital based assessment of the XC functionals of the density functional theory employed, and an understanding of the chemical bonding mechanisms within the species. Finally, the spectroscopic strengths calculated using outer valence Green’s function theory are compared against those derived from our EMS measurements.

(Some figures in this article are in colour only in the electronic version)

⁶ Permanent address: Faculty of Science, Shahid Bahonar University of Kerman, Kerman, Iran.

1. Introduction

Computational molecular design is becoming an ever increasing part of rational drug design. This inherently requires an accurate understanding of the interactions between small molecules and proteins, and their important functional groups, at the molecular level to determine molecular properties and mathematical parameters which can be used to describe a molecule, known as descriptors. These descriptors can then be used to develop quantitative structure activity relationship (QSAR) models that are used to identify new molecules which are likely to exhibit desired characteristics. McCoy and Sykes [1] quite recently have reported a novel technique for the generation of molecular descriptors based on *ab initio* calculated momentum distributions. Electron momentum spectroscopy has the unique ability of being able to directly probe the molecular wavefunction in momentum space [2], and can therefore elucidate the quality of various theoretical quantum mechanical methods, and the validity of employing a momentum space descriptor approach obtained from *ab initio* calculations.

At Flinders University, we are using electron momentum spectroscopy (EMS) to study the behaviour of the geometrically similar molecules, bicyclo[2.2.2]octa-2,5-dione ($C_8H_{12}O_2$, refer to as (1)), bicyclo[2.2.1]hepta-2,5-dione (BCHD, $C_7H_8O_2$, (2)) and stella-2,6-dione ($C_8H_8O_2$, (3)) [3], which are diketone derivatives of bicyclo[2.2.2]octane, norbornane (NBA) and stellane [4], respectively. Here the strain within the respective molecules increases as the system goes from (1) to (3), and we are interested in studying the effects of this increased strain on the bonding mechanisms within the molecules. Additionally, these molecules are interesting as they have previously demonstrated that the strength of the through-bond interaction is important for long-range electron-transfer processes [4]. These diketones have been quite recently synthesized at the University of Heidelberg, and in this report we outline our EMS and photoelectron spectroscopy (PES) results of the second molecule in the geometric series, BCHD (see figure 1).

In the following section, the high resolution electron momentum spectroscopy (HREMS) [5] experimental apparatus and measurement techniques will be briefly described, followed by an outline of our theoretical methods. We will then present and discuss our results and finally proceed to summarize the conclusions drawn from this study.

2. Experimental details

In EMS, we perform the kinematically complete electron impact ionization experiment of the target of interest (see figure 2). This can be described by

$$e_0(\mathbf{k}_0, E_0) + T \rightarrow T_i^+ + e_s(\mathbf{k}_s, E_s) + e_f(\mathbf{k}_f, E_f), \quad (1)$$

where T is the molecular target, e with the subscripts 0, s and f represents the initial, slow and fast electrons respectively, which have momentum \mathbf{k} and energy E . The slow and fast electron notation are used due to the indistinguishable nature of the electrons after the collision. Here we note, from the conservation of energy,

$$E_0 = \epsilon_f + E_s + E_f \quad (2)$$

where ϵ_f is the binding energy of the ejected electron. We perform our EMS measurements under symmetric non-coplanar kinematic conditions, such that the polar angles that the slow electron and the fast electron make with respect to the incident beam direction are equal ($\theta_s = \theta_f = 45^\circ$), and an azimuthal angle, ϕ , is varied. Here the energies of the detected electrons are also equal ($E_s = E_f = 750$ eV). Under these symmetric non-coplanar conditions

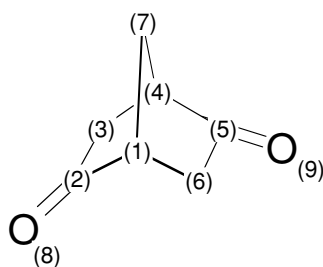


Figure 1. Structural representation of bicyclo[2.2.1]hepta-2,5-dione.

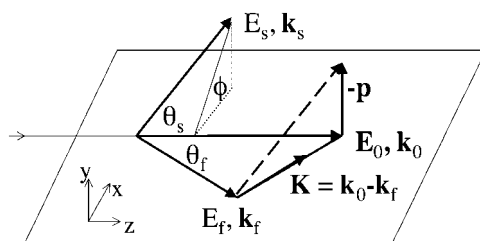


Figure 2. A schematic diagram showing the kinematics of the EMS experiment.

and within the binary encounter approximation regime, scanning over a range of azimuthal angles, ϕ , is equivalent to scanning over the momenta of the bound electron, p , as [2]

$$p = \left[(2k_s \cos \theta - k_0)^2 + 4k_s^2 \sin^2 \theta \sin^2 \left(\frac{\phi}{2} \right) \right]^{\frac{1}{2}}. \quad (3)$$

Equation (3) follows from the conservation of momentum and a consideration of the scattering kinematics in figure 2.

The 15 outer-most valence molecular orbitals of BCHD in the electronic ground state were investigated over two independent experimental runs using the Flinders symmetric non-coplanar HREMS spectrometer (see figure 3). Briefly, describing this spectrometer, we have a hemispherical electron monochromator producing an electron beam, with well-defined energy, $E_0 = 1500 \text{ eV} + \epsilon_f$, which is housed in its own differentially pumped chamber. The purpose of this monochromator is to produce a beam of good flux (typically 20–30 μA into the interaction region), and of relatively narrow energy width ($\sim 0.3 \text{ eV}$ FWHM). The electrons are produced by thermionic emission from a tungsten hairpin filament, and collimated and transported into the interaction region, using a series of cylindrical-symmetry lenses and apertures. The incident electron beam is crossed at 90° to the target molecular beam (which is out of page in figure 3) in the main chamber, which is pumped by a 6 inch diffusion pump. Here the high-purity BCHD sample ($>99.9\%$), which was prepared from norbornadiene [6–8], is released into the interaction region via a capillary array, which is controlled by a variable leak valve. Note that the BCHD driving pressure is chosen to ensure that there is no significant clustering by supersonic expansion. Apertures and slits are cut into the interaction region, which is differentially pumped by a 700 l s^{-1} diffstack, for the incident, scattered and ejected beams. The main chamber is always maintained at a background pressure of less than 2×10^{-5} Torr, enabling the generation of sufficient coincidence count rates, but being low enough to operate the high voltages needed for the detectors.

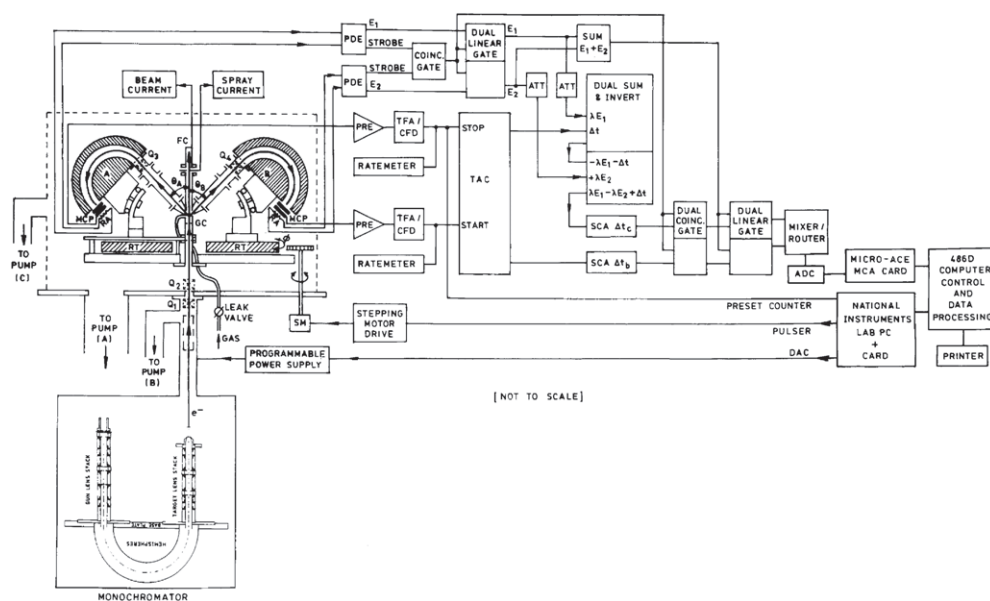


Figure 3. A schematic diagram of the symmetric non-coplanar HREMS spectrometer based at Flinders.

The scattered and ejected electrons are energy analysed using the respective hemispherical analysers. The passed electrons are detected by the microchannel plate (MCP)/resistive anode (RA) assemblies. Each of the MCP/RA assemblies, produce a fast and a slow pulse when an electron is detected. These correspond to the timing and position/energy signals respectively. The timing pulses from each of the hemispherical analysers are used in conjunction with a time-to-amplitude converter (TAC) to determine if the detected electrons originate from the same ionization event [5]. The remaining circuitry is responsible for determining the number of coincidence counts as a function of the binding energy of a given target electron momentum, at each respective value of $\phi(p)$ of interest in this work.

The coincidence energy resolution of the spectrometer was typically 0.50 eV (FWHM) in the present studies, as determined from binding energy measurements on helium. The angular resolution of the apparatus is 1.2° (FWHM), as determined from the argon $3p$ angular correlation.

Photoelectron spectroscopy (PES) measurements, using a He(I) source, were made at Heidelberg as a part of the present study. The PES measurements were recorded on a PS 18 instrument from Perkin Elmer at 27°C . This spectrometer was calibrated with Ar (15.76 and 15.94 eV) and Xe (12.13 and 13.44 eV), with a resolution of 20 meV being obtained for the $^2P_{3/2}$ Ar line.

3. Theory and computational details

In high momentum transfer ($e,2e$) collisions we employ the binary-encounter approximation, such that the initial N -electron wavefunction is equated to the product of the final residual ion ($N - 1$)-electron wavefunction and the one-electron wavefunction corresponding to the ejected electron. Furthermore, by employing the plane-wave impulse approximation (PWIA),

the EMS cross section for randomly oriented molecules, in unresolved rotational and vibrational states for ionization through the f th ionization channel is given by

$$\sigma_f = K \int d\Omega |\langle \mathbf{p} \Psi_f^{N-1} | \Psi_i^N \rangle|^2, \quad (4)$$

where K is a kinematical factor (which is approximately a constant for the present symmetric, non-coplanar conditions), Ψ_f^{N-1} is the residual ion ($N-1$)-electron many-body wavefunction, Ψ_i^N is the N -electron many-body ground state wavefunction and \mathbf{p} is a plane wave. Here the integration performs the spherical averaging of the initial rotational states. We also note that the averaging over initial vibrational states is incorporated by considering the orbitals of the molecule at their equilibrium geometry, generated for the optimized geometry, whilst closure eliminates the final rotational and vibrational state dependence [2]. The momentum space target-ion overlap can be directly evaluated using a configuration interaction (CI). Using a method analogous to that developed by Deleuze *et al* [9] to compute photoionization intensities, the transition amplitude of equation (4) can be recast in terms of a structure factor derived from the Fourier transform of a Dyson spin-orbital for the ionization channel under consideration, such that

$$\sigma_f = K \int d\Omega |g_f(\omega, \vec{p})|^2, \quad (5)$$

where the corresponding coordinate space representation of the Dyson spin-orbital, $g_f(\mathbf{x})$, is defined as the partial overlap between the neutral N -electron ground state and final ($N-1$)-electron ion state,

$$g_f(\mathbf{x}) = \sqrt{N} \int \Psi_f^{N-1}(\mathbf{x}_1, \mathbf{x}_2, \dots, \mathbf{x}_{N-1}) \Psi_i^N(\mathbf{x}_1, \mathbf{x}_2, \dots, \mathbf{x}_N) d\mathbf{x}_1 d\mathbf{x}_2 \dots d\mathbf{x}_{N-1}. \quad (6)$$

Here ω is a spin coordinate and $\mathbf{x}_i = (\omega_i, \vec{r}_i)$ represents the spin-space coordinate of the i th electron. Expanding the spin-free Dyson orbital in a canonical MO basis, the target-ion overlap in equation (4) can be replaced by a structure factor derived as the Fourier transform of the associated Hartree-Fock or Kohn-Sham ground state defined as the norm of the Dyson orbital pertaining to the ionization channel f :

$$\sigma_f = K \sum_{j'} S_{j'}^{(f)} \int d\Omega |\phi_{j'}(\vec{p})|^2. \quad (7)$$

Here the Feynman-Dyson transition amplitudes for ion state f and orbital j' are given by

$$S_{j'}^{(f)} = |\langle \Psi_f^{N-1} | a_{j'} | \Psi_0^N \rangle|^2, \quad (8)$$

where $a_{j'}$ corresponds to the annihilation operator for an electron in the j' th molecular orbital in the second quantization treatment [10]. By further neglecting the electronic relaxation of molecular orbitals, i.e. assuming that the f th ionization channel is dominated by contributions through the j th molecular orbital, which in turn predominantly ionizes through the f th ionization channel, the EMS cross section reduces to

$$\sigma_f \approx K \Gamma_f \int d\Omega |\phi_j(\vec{p})|^2, \quad (9)$$

where the spectroscopic strength of the residual state f is given by

$$\Gamma_f = \sum_{j'} S_{j'}^{(f)} \quad (10)$$

$$\approx S_j^{(f)}. \quad (11)$$

Here the fraction of intensity that is lost into secondary shake-up processes is equal to $1 - \Gamma_f$ [11], such that this approximation is only valid for states whose shake-up states difference in energies are comparable to the experimental energy resolution and that there are no other major shake ups from other states within the experimental energy range. Typically the benchmark for the validity of the one electron orbital ionization approximation is given by spectroscopic strengths, $\Gamma_f > 0.85$ [12]. The Feynman–Dyson transition amplitudes and spectroscopic strengths satisfy the following sum rules,

$$\sum_f S_j^{(f)} = 1 \quad (12)$$

$$\sum_f \Gamma_f = N, \quad (13)$$

provided all ionization channels are identified. The implementation of equation (9) is carried out in the AMOLD codes of McCarthy and Weigold [13] for HF and DFT wavefunctions.

The dependence of the cross section on the absolute square of the many-body wavefunction (as can be seen in equation (9)) provides a means to experimentally determine the accuracy of various computational chemistry methods on an orbital by orbital basis, under the PWIA. In this study, we concentrate on the exchange correlation (XC) functionals incorporated into a couple of commonly used DFT models. Specifically, the Becke and Perdew (BP) [14–16] generalized gradient approximation (GGA) XC functional and the Becke [17] three parameter hybrid functional, with the non-local correlation of Lee, Yang and Parr [18] (B3LYP) XC functional are employed in this study for the orbital momentum distribution calculations. The corresponding calculations are also performed using the restricted Hartree–Fock (RHF) model, which does not include any correlation effects but fully includes the exchange energy to generate a reference point. Our RHF and DFT calculations on the orbital momentum distributions of the species have been performed using the triple zeta quality valence polarized (TZVP) basis of Godbout *et al* [19], with the geometry being optimized using the B3LYP/TZVP model. These calculations have been employed using the DGauss package of UniChem [20, 21] (for the BP/TZVP results) and also the GAMESS [22] and Gaussian 03 [23] suites of programs (for B3LYP/TZVP and RHF/TZVP results). The outer valence Green’s Function (OVGF) calculations [23] were also performed at the B3LYP/TZVP optimized geometry using Dunning’s correlation consistent polarized valence basis of double zeta quality (cc-pVDZ) [24].

The accuracy of DFT calculated orbital energies has traditionally been found to be in poor agreement with experimental PES and EMS binding energy measurements, as Koopmans’ theorem [25] does not hold for Kohn–Sham orbital energies. However, recent developments in DFT using the ‘meta-Koopmans’ theorem [26–29], an analogue of Koopmans’ theorem for DFT, can generate vertical ionization potential (VIP) energies of molecular species with an accuracy up to 0.2 eV, using the recently developed orbital-dependent statistical average of different model orbital potentials (SAOP) [27, 30, 31] method, which is particularly successful in modelling the XC functional [28]. The SAOP potential provides quite good VIPs, including those from the inner valence region, provided that there are no appreciable shake-up satellites [29]. This is generally the case for orbitals with binding energies below 20 eV, i.e. the outermost valence region, unless their are unusual shake-ups (as is the case for ozone, formamide, CS₂, etc) [29]. SAOP has been embedded in the Amsterdam Density Functional (ADF) suite of programs [32]. The present work computes the binding energies of BCHD using the SAOP/TZ2P model. The TZ2P basis set is a Slater type triple zeta plus double polarization basis set [33], which is the closest basis set to the Gaussian TZVP basis set [20] we also

Table 1. The optimized geometries of BCHD, compared to the optimized geometry of norbornane (NBA). Refer to figure 1 for the numbering sequence.

| Parameter | B3LYP/TZVP | MP2/TZVP | RHF/TZVP | NBA B3LYP/cc-pVTZ ^a |
|-------------------------|------------|----------|----------|--------------------------------|
| C(1)–C(2) (Å) | 1.527 | 1.530 | 1.520 | 1.543 |
| C(1)–C(6) (Å) | 1.554 | 1.556 | 1.547 | 1.543 |
| C(1)–C(7) (Å) | 1.550 | 1.550 | 1.543 | 1.540 |
| C(2)–C(3) (Å) | 1.539 | 1.540 | 1.531 | 1.562 |
| C(2)–O(8) (Å) | 1.204 | 1.207 | 1.182 | – |
| C(1)–H (Å) | 1.088 | 1.088 | 1.079 | 1.089 |
| C(3)–H (Å) | 1.092 | 1.092 | 1.084 | 1.091 |
| C(3)–H (Å) | 1.095 | 1.092 | 1.086 | – |
| C(7)–H (Å) | 1.093 | 1.093 | 1.085 | 1.091 |
| C(2)–C(6) (Å) | 2.455 | 2.450 | 2.447 | 2.516 |
| C(2)–C(3)–C(4) (°) | 102.495 | 102.497 | 102.322 | 103.08 |
| C(1)–C(7)–C(4) (°) | 95.406 | 95.963 | 95.296 | 94.42 |
| C(3)–C(4)–C(5) (°) | 105.586 | 105.107 | 105.860 | 108.47 |
| C(2)–C(1)–C(7) (°) | 101.164 | 101.245 | 101.269 | 101.54 |
| C(3)–C(2)–O(8) (°) | 126.581 | 126.591 | 126.433 | – |
| H–C(3)–H (°) | 107.669 | 108.367 | 107.974 | 107.33 |
| H–C(7)–H (°) | 108.785 | 109.117 | 108.686 | 108.95 |
| C(5)–C(4)–C(3)–C(2) (°) | 69.276 | 69.563 | 69.412 | – |
| C(4)–C(3)–C(2)–O(8) (°) | –178.370 | –178.639 | –179.129 | – |
| C(7)–C(1)–C(2)–O(8) (°) | –147.154 | –147.060 | –146.377 | – |
| C(7)–C(4)–C(3)–C(2) (°) | –35.463 | –35.197 | –35.215 | – |
| μ/D | 2.952 | 3.346 | 3.131 | 0.089 |

^a [35].

employed. To make a comparison, outer-valence Green's function (OVGF) calculations [34] which have been used to calculate binding energies of other molecules such as norbornane [35] are also carried out for BCHD in the present study, in this case using the Gaussian 03 [23] suite of programs.

4. Results and discussion

4.1. Geometrical and electronic information

The ground electronic state (X^1A) of bicyclo[2.2.1]hepta-2,5-dione ($C_7H_8O_2$) has a C_2 symmetry with 33 doubly occupied molecular orbitals (MOs). Using the B3LYP/TZVP model, the outer valence shell configuration is given by

$$\dots (6a)^2(5b)^2(7a)^2(6b)^2(7b)^2(8a)^2(8b)^2(9a)^2(9b)^2(10b)^2(10a)^2(11b)^2(11a)^2(12a)^2(12b)^2.$$

This configuration of the outer valence MOs may alter due to the orbital-dependent XC energy involved. As the species was only recently synthesized, there are no comprehensive experimental data available for comparison. As a result, three quantum-mechanical models including B3LYP/TZVP, MP2/TZVP and RHF/TZVP have been employed to produce a reliable geometry of the ground state of BCHD. Table 1 gives the geometry of the BCHD molecule (X^1A), optimized using the models mentioned above, together with the related geometry parameters of norbornane (NBA) [35], which possesses the same bicyclic framework as BCHD but with the C–H bonds on the $C_{(2)}$ and $C_{(5)}$ atoms being replaced by C=O bonds, respectively. As shown in this table, the geometrical parameters given by the B3LYP/TZVP

Table 2. Experimental and theoretical binding energies (eV) for the outer valence orbitals of BCHD. Note that the reported energies for the B3LYP/TZVP and RHF/TZVP models are those obtained through GAMESS [22].

| Peak | Label (symbol) | RHF/TZVP ^a | BP/TZVP ^a | B3LYP/TZVP ^a | SAOP/TZ2P ^a | OVGf/cc-pVTZ ^a | HAM/3 ^b | PES ^b | Present PES | Present EMS |
|------|----------------|-----------------------|----------------------|-------------------------|------------------------|----------------------------|--------------------|------------------|-------------|-------------|
| 1 | 12b | 11.143 | 5.97 | 7.064 | 10.42 | 9.380 (0.903) | 9.40 | 9.47 | ~9.4 |]] |
| | 12a | 11.162 | 6.00 | 7.080 | 10.43 | 9.375 (0.904) ^c | 9.46 | 9.63 | ~9.5 |]]9.45 |
| 2 | 11a | 13.214 | 8.62 | 9.614 | 12.89 | 11.951 (0.895) | 11.52 | |]] |]] |
| | 11b | 13.287 | 8.72 | 9.682 | 12.88 ^c | 11.961 (0.901) | | |]]~12.1 |]]12.10 |
| 3 | 10a | 14.332 | 9.33 | 10.398 | 13.45 | 12.826 (0.909) | | | ~12.9 |]] |
| | 10b | 14.493 | 9.47 | 10.542 | 13.61 | 13.033 (0.902) | | | ~13.0 |]]12.95 |
| 4 | 9b | 14.972 | 9.67 | 10.819 | 13.87 | 13.418 (0.907) | | | ~13.3 |]]13.30 |
| 5 | 9a | 15.541 | 9.91 | 11.143 | 14.14 | 13.696 (0.901) | | | ~13.6 |]]13.60 |
| 6 | 8a | 16.009 ^c | 10.02 | 11.226 | 14.29 | 14.000 (0.889) | | | ~13.9 |]]13.9 |
| 7 | 8b | 15.905 | 10.34 | 11.559 | 14.58 | 14.274 (0.904) | | | ~14.1 |]] |
| | 7b | 16.243 | 10.57 | 11.802 | 14.78 | 14.462 (0.902) | | | ~14.4 |]]14.4 |
| 8 | 6b | 17.135 | 10.87 | 12.169 | 15.09 | 15.000 (0.889) | | | ~15.0 |]]15.1 |
| 9 | 7a | 17.747 | 11.97 | 13.222 | 16.15 | 16.073 (0.898) | | | ~16.3 |]] |
| | 5b | 18.629 | 12.09 | 13.434 | 16.34 | 16.554 (0.889) | | | ~16.6 |]]16.60 |
| | 6a | 19.094 | 12.29 | 13.666 | 16.57 | 17.008 (0.889) | | | ~16.9 |]] |

^a Calculation performed at B3LYP/TZVP optimized geometry.^b [38].^c Flipped orbital.

and MP2/TZVP models agree very well, indicating that the XC energy is quite sensitive to the bond stretch motions.

The calculated bond angles for the bicyclic carbon frame, which do not apparently deviate from their NBA counterparts, are consistent among the models. For the \angle HCHs, the MP2/TZVP model seems to overestimate the angles when compared to the DFT-based B3LYP model and the RHF model, which generate consistent results. Compared to the geometrical parameters of NBA, which were calculated using the B3LYP model with a similar basis set of cc-pVTZ, the bicyclic carbon framework of BCHD does not exhibit any significant changes, due to the addition of the keto groups. However, a small relaxation in the geometry is observed. For example, the four independent C–C single bonds in BCHD are closer in their bond lengths than those of the NBA in which the C₍₂₎–C₍₃₎ bond is apparently longer than the other C–C bonds in the molecule [35]. The two C–C bonds which directly connect to the C=O groups, i.e., C₍₁₎–C₍₂₎ and C₍₂₎–C₍₃₎ are slightly reduced to accommodate the CO groups. This is reflected in the BCHD bond angles where \angle C₍₂₎C₍₃₎C₍₄₎ and \angle C₍₃₎C₍₄₎C₍₅₎ are reduced and the bridge angle, \angle C₍₁₎C₍₇₎C₍₄₎, is slightly enlarged.

4.2. Binding energy spectra

Representative EMS binding-energy spectra of BCHD, for energies $\epsilon_f = 7$ –18 eV, and at azimuthal angles $\phi = 0^\circ$ and $\phi = 10^\circ$ are presented in figure 4. A least-squares method is used to fit nine Gaussian functions, whose respective peaks are assigned at the binding energy of the corresponding PES measurement (see table 2), or average binding energy of the

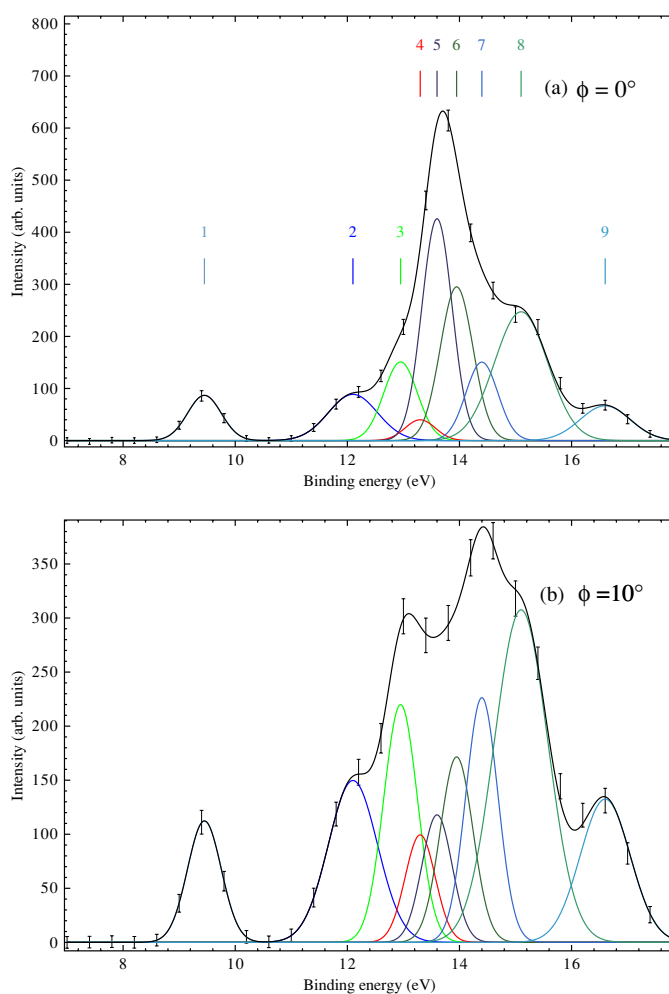


Figure 4. The EMS binding energy spectra for azimuthal angles (a) $\phi = 0^\circ$ and (b) $\phi = 10^\circ$. The numbers indicate the individual Gaussians used in the spectral deconvolution.

unresolved orbitals, to each spectra in order to extract the required momentum distributions. These peaks are chosen to ensure that a physically reasonable fit to the binding energy spectra can be achieved at all binding energies, a task which is aided by the EMS sensitivity to orbital symmetries. Note further that the widths of the respective Gaussian functions were fixed at values representing a convolution of the EMS experimental energy resolution and the respective natural (Franck–Condon) line widths of the various orbitals. These latter widths were taken from our PES data (see later). We can see from figure 4 that the overall fit to the binding energy spectra (solid line representing the envelope of the fit) is in excellent agreement with the experimental measurements at both azimuthal angles.

Figure 4(a) gives the binding energy spectrum at $\phi = 0^\circ$ ($p \approx 0.03$ au), where the dominant contributions are from the s electrons, whereas figure 4(b) gives a spectrum at $\phi = 10^\circ$ ($p \approx 0.92$ au), which is dominated by contributions from the p, d, f...-AOs. BCHD consists of atoms that are in the first row of the periodic table, and therefore the d and f-AOs are

Table 3. Peak heights (arbitrary units) from our $\phi = 0^\circ$ and $\phi = 10^\circ$ binding energy spectra and their suggested bonding character. Details on our fitting procedure can be found in the text.

| Peak | $I(\phi = 0^\circ)$ | $I(\phi = 10^\circ)$ | $\Delta I(10-0)$ | Suggested bonding character |
|------|---------------------|----------------------|------------------|-----------------------------|
| 1 | 86.837 | 112.343 | 25.507 | s,p |
| 2 | 88.786 | 149.706 | 60.920 | s,p |
| 3 | 150.993 | 219.943 | 68.950 | s, strong p |
| 4 | 39.935 | 99.444 | 59.509 | Weak p |
| 5 | 426.003 | 117.949 | -308.054 | Strong s |
| 6 | 295.284 | 171.599 | -123.685 | Strong s, p |
| 7 | 150.692 | 226.394 | 75.702 | s, strong p |
| 8 | 247.257 | 307.595 | 60.338 | Strong s, strong p |
| 9 | 66.755 | 132.510 | 65.755 | s,p |

unoccupied, and consequently cannot significantly participate in the bonding. Consequently, the $\phi = 10^\circ$ AO contributions for BCHD can essentially be thought of as the contribution from the p-electrons. Comparing the binding energy spectra in figures 4(a) and (b), we see that the fifth peak, which corresponds to the 9a MO, has a significant reduction in observed intensity (I) in going from $\phi = 0^\circ$ ($I = 426.0$) to $\phi = 10^\circ$ ($I = 117.9$). As a result, the 9a MO corresponding to this peak exhibits ‘s-like’ symmetry (the bonding is dominated by s-electrons). On the other hand, the intensity of the 9b MO (peak 4) increases significantly at the higher momentum value, indicating ‘p-like’ symmetry. This change in symmetry is crucial for a unique deconvolution of the various peaks being obtained, particularly in regions where there is a fair degree of energy overlap between the respective MOs. It is noted, however, that most of the other outer valence MOs exhibit a combination of s and p electron contributions, which leads to the observation of ‘hybrid-like’ MOs. The suggested bonding character information obtained from the binding energy spectral intensities is given in table 3.

The outer valence Green’s function and density functional theory calculated binding energies of BCHD are presented in table 2. Here we note that the SAOP method produces quite good agreement with the experimental results. This result is particularly good considering the poor agreement observed between the experimental results and those obtained using other density functional methods. However, the OVGf results are still quite clearly found to be in the best agreement with the experimentally measured binding energies over the entire energy range considered. Indeed, because of this good agreement, the OVGf results were particularly useful in the interpretation of both our EMS and PES binding energy spectra and, as a consequence, our momentum distributions.

The He(I) photoelectron spectroscopy of BCHD has also been measured in the present study. These data are presented in figure 5(a) and upon comparison with the EMS binding energy spectra for $\phi = 0^\circ + 10^\circ$ (figure 5(b)), we observe good qualitative agreement, although the superior energy resolution of the PES data is apparent. Note also that there are some variations in the magnitude of the peak intensities, between the PES and EMS spectra. This has been observed many times in PES and EMS spectra with the origin for this difference being well discussed in Weigold and McCarthy [2].

4.3. Orbital momentum distributions

Using the peak areas of the respective fitted Gaussians, from the measured binding energy spectra, the individual orbital momentum distributions (MDs) for each of the outer valence molecular orbitals can be derived. Here the experimental measurements are put on an absolute

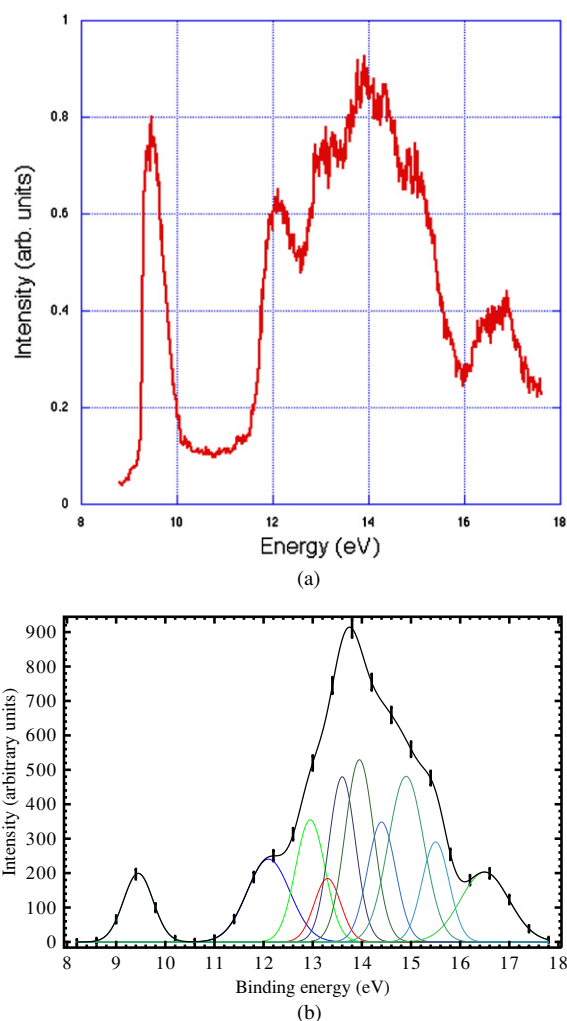


Figure 5. (a) The present He(I) PES binding energy spectra. (b) The EMS binding energy spectra for $\phi = 0^\circ + 10^\circ$.

scale by normalization to the PWIA-BP/TZVP calculation, by considering the ratio of the sum of the PWIA cross sections at all recovered ϕ for all the molecular orbitals considered to the total area under the binding energy spectra at the corresponding ϕ . We then compare the normalized experimental measurements to the theoretical PWIA calculations, which use wavefunctions generated at the BP/TZVP, B3LYP/TZVP and RHF/TZVP levels for a selection of the molecular orbitals in the outer valence shell.

Like norbornane [35, 36], BCHD does not possess a molecular plane where all component atoms lie. It is therefore expected that the MOs and the bonding of the species can only be looked at locally, with some MOs possessing bonding characters which are not purely σ or π bonds, rather, the orbital MDs are likely to exhibit hybrid or mixed s- and/or p-like MOs. This is consistent with what we saw in our binding energy spectra and which was summarized in table 3.

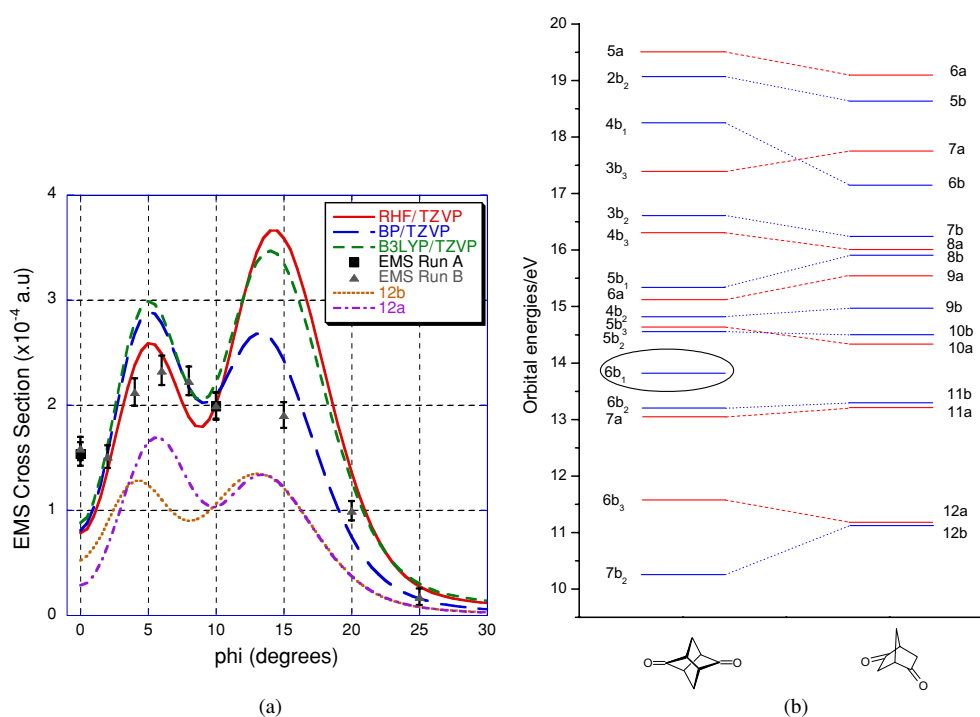


Figure 6. The 1500 eV symmetric non-coplanar momentum density for the 12b + 12a orbitals of BCHD ($\epsilon_f = 9.45$ eV). The experimental measurements for run A (■) and run B (▲) are compared against PWIA calculations using RHF (—), BP (---) and B3LYP (···) model chemistries. Also shown are the individual 12b (···) and 12a (···) results for the BP model chemistry. (b) Valence orbital correlation diagram for stella-2,6-dione and bicyclo[2.2.1]hepta-2,5-dione.

The first momentum density we consider is for the 12b + 12a orbitals (see figure 6(a)). Here orbital 12b which is the highest-occupied molecular orbital (HOMO) and orbital 12a, which is the next highest-occupied molecular orbital (NHOMO), are unresolved due to the closeness in their binding energies. The general agreement between the observed and simulated orbital MDs for this orbital pair superposition is only fair, being quite marginal in the very low momentum region corresponding to $\phi < 2^\circ$ and being only somewhat better in the region corresponding to $\phi = 10^\circ$ – 20° . We note that the observed ‘turn-up’ in the experimental flux for $\phi \leq 2^\circ$ is not unique to this molecule, having been observed in the HOMO of norbornane [11] by Knippenberg *et al* and in the HOMO of O₂ by Ning *et al* [37]. Possible explanations for the cause of this phenomenon can be found in these papers and so we do not repeat that detail here. Somewhat surprisingly, the RHF/TZVP model appears to generate the best agreement with the experimental MD for $\phi \leq 10^\circ$. On the other hand, in the higher momentum region, only the BP/TZVP model approaches a physical description for the experimentally observed behaviour, although here we note that the interpolation between $\phi = 10^\circ$ and $\phi = 15^\circ$ is not unique. Nevertheless, we can draw theoretical insight from figure 6(a). First, all the models underestimate the s-component in the bonding of the HOMO and NHOMO, i.e., the diketo groups of C=O. The experimentally observed s-component is nearly twice as much as that simulated. Second, there are really too few experimental points in the region of $\phi = 10^\circ$ – 20° to quantitatively assess the theoretical models employed. Specifically, there is only a single

point at $\phi = 15^\circ$, which is somewhat overestimated by the BP/TZVP model and significantly overestimated by all the other theoretical calculations. This is one limitation in performing the measurements well in advance of the calculations, particularly when only a small amount of the sample is available for study. In such circumstances, problematic regions of momentum for the theory may be experimentally missed, as what has happened here.

The consistent agreement between the magnitudes of the experimental MD measurements and the theoretical MD calculations, particularly in the low momentum region nonetheless suggests that the EMS spectroscopic factors (see equation (9)) for both these orbitals are close to unity, which is in good accord with our OVGf results (see table 2).

The multiple peaks in the combined HOMO and NHOMO MDs in figure 6(a) indicate that at least two 2p electrons participate in the bonding. The local minimum observed in all theoretical models (and suggested by the experiment) in the region about $\phi \sim 8^\circ$ further indicates that the two 2p electrons are located on different atoms, which have significant separation, such that there is a minimal overlap between the 2p atomic orbitals. The experimental orbital MDs of the combined HOMO and NHOMO exhibit a combination of s and p electron contributions to the bonding, as reflected by the small local maximum in the low momentum region ($\phi = 0^\circ$), which is not replicated in the theoretical calculations. This supports the notion that there is substantial interaction between the 2p electrons and the C–C σ frame. To study the orbital MDs of the HOMO and the NHOMO individually, the theoretical orbital MDs of the individual HOMO (12b) and NHOMO (12a) are also presented in the same figure. Although we only present the orbital MDs at the BP/TZVP level, all the theoretical calculations are consistent with respect to the observed bonding nature. Here we see that the 2p electrons in the low momentum region have stronger contributions from the NHOMO, whereas the 2p electrons for the higher momentum regions ($10^\circ \leq \phi \leq 30^\circ$) have approximately equal contributions to the 12a + 12b MD. From the electronic structural point of view, the HOMO and the NHOMO of BCHD are dominated by the contributions from the 2p lone pairs of the O atoms. Such an observation is not very different from the HOMO ($7b_2$) and NHOMO ($6b_3$) of stella-2,6-dione [3] in this series. Nonetheless there are some quantitative differences between the HOMO and NHOMO in stella-2,6-dione and BCHD. To illustrate this point consider in figure 6(b) the valence orbital correlation diagram for stella-2,6-dione and BCHD. The most interesting observation in this diagram is the large split of the 2p lone pair combinations (n_+ , n_-) at the oxygen centres of stella-2,6-dione ($7b_2/6b_3$), as compared to those of BCHD (12b/12a). The main reason for that is a stronger interaction between the $b_2(n_+)$ linear combinations of the oxygen lone pairs of stella-2,6-dione and a $b_2(\sigma)$ orbital as compared to $b_3(n_-)$ $b_3(\sigma)$. The $b_2(\sigma)$ orbital is mainly localized at the central six-membered ring, oriented perpendicular to the two CO groups. For BCHD a σ -orbital which interacts mainly with only one linear combination of the oxygen 2p orbitals is missing due to the lower symmetry of BCHD. In addition, in stella-2,6-dione there is a significant C–C σ orbital contribution to both the HOMO and the NHOMO whereas in BCHD the C–C σ orbital contribution is much more predominant in the NHOMO compared to the HOMO. However due to the high symmetry (D_{2d}) of stella-2,6-dione, in which the diketone groups are located symmetrically resulting in a zero molecular dipole moment, the orbital MDs of the HOMO and the NHOMO in stella-2,6-dione are qualitatively similar. The molecular symmetry of BCHD is C_2 with a nonzero molecular dipole moment as seen in table 1. Consequently, BCHD possesses a more unbalanced contribution to the HOMO and NHOMO MDs. Nevertheless, the overall bonding nature of the 2p electrons does not change substantially between BCHD and stelladione.

The combined 11a + 11b orbital MDs, which are shown in figure 7, show a hybrid orbital that is dominated by a strong ‘p-like’ symmetry contribution. Here we observe that all

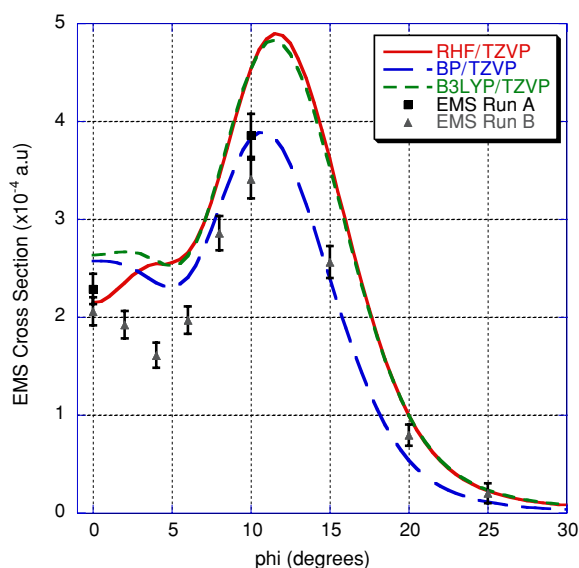


Figure 7. The 1500 eV symmetric non-coplanar momentum density for the 11a + 11b orbitals of BCHD ($\epsilon_f = 12.1$ eV). The experimental measurements for run A (■) and run B (▲) are compared against PWIA calculations using RHF (—), BP (---) and B3LYP (- · -) model chemistries.

theoretical methods are reasonably consistent in predicting the profile of the combined orbital MDs. However, we note that the reported magnitudes vary significantly across the azimuthal angular range at the different theoretical levels. In the momentum region $\phi < 7.5^\circ$ none of the calculations generate quantitative agreement with the experimental data, particularly for $\phi < 6^\circ$ where all the theoretical calculations over estimate the cross section magnitude. In the large momentum region, $\phi \geq 10^\circ$ the BP/TZVP model generates best overall agreement with experiment, although it also exhibits further limitations here. Nonetheless, on balance we believe that figure 7 suggests that the BP/TZVP model chemistry provides the best shape and magnitude agreement with the measurement for the 11a + 11b orbital MD.

The spectral deconvolution in the binding energy range $\epsilon_f = 13.3$ – 14.8 eV requires extreme care, due to the relative closeness, number of states and potential overlap in this region. To combat this we initially proceed to combine the 9b, 9a, 8a, 8b and 7b orbitals which occur in this binding energy region, with the corresponding combined orbital MDs being shown in figure 8. This procedure is done to preserve the integrity of the fitting procedure, although it invariably leads to a loss in physical information. This is certainly the case here where it is not easy to definitively assess which of the model chemistries gives best agreement with the data. Figure 8 suggests that the BP/TZVP model might provide the most physical description for $\phi < 15^\circ$, but thereafter underestimates the magnitude of the MD. The B3LYP/TZVP and RHF/TZVP calculation generate fair agreement, except in the range $5^\circ < \phi < 15^\circ$. To try and extract further information from the combined orbital MDs, we consider the individually de-convoluted states, which have been spectrally assigned taking the observed orbital symmetries into account, as well as utilizing our PES data and binding energy calculations.

The first interesting MD from the combined binding energy region corresponds to the 9a MO (see figure 9). Here we observe that this orbital shows dominant ‘s-like’ symmetry,

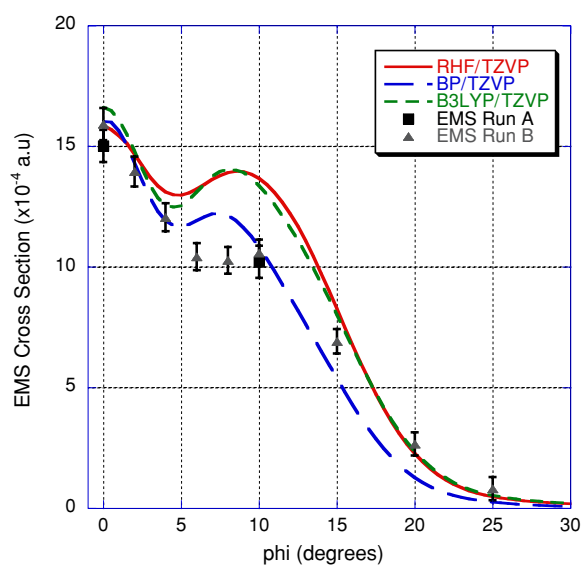


Figure 8. The 1500 eV symmetric non-coplanar momentum density for the combined 9b, 9a, 8a, 8b and 7b orbitals of BCHD ($\epsilon_f = 13.2\text{--}14.8$ eV). The experimental measurements for run A (■) and run B (▲) are compared against PWIA calculations using RHF (—), BP (---) and B3LYP (- - -) model chemistries.

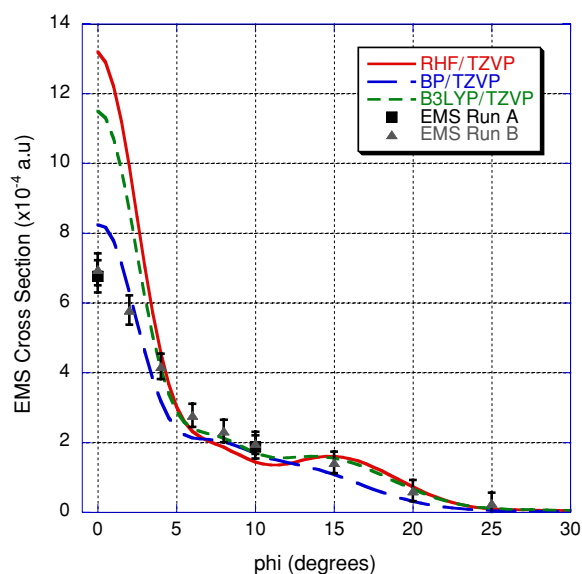


Figure 9. The 1500 eV symmetric non-coplanar momentum density for the 9a orbital of BCHD ($\epsilon_f = 13.6$ eV). The experimental measurements for run A (■) and run B (▲) are compared against PWIA calculations using RHF (—), BP (---) and B3LYP (- - -) model chemistries.

as predicted from the binding energy spectra (peak 5). It is noted that all the theoretical MDs are consistent in this regard, although significant discrepancies between the magnitudes

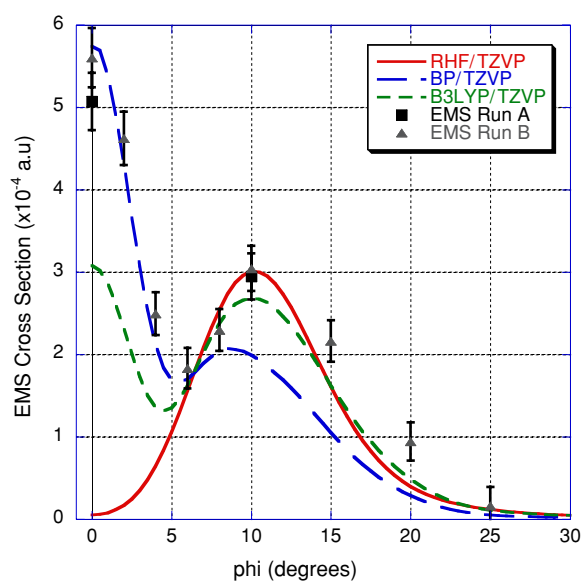


Figure 10. The 1500 eV symmetric non-coplanar momentum density for the 8a orbital of BCHD ($\epsilon_f = 13.95$ eV). The experimental measurements for run A (■) and run B (▲) are compared against PWIA calculations using RHF (—), BP (---) and B3LYP (- - -) model chemistries.

of the theoretical values for $\phi \leq 6^\circ$ are observed. Here, the BP/TZVP model is found to accurately reproduce the experimental MD data for this MO and this enables us to assign an EMS spectroscopic factor, at $\epsilon_f = 13.6$ eV, of value ≈ 1 . This result is also consistent with those from our OVGf calculation (see table 2). All the B3LYP/TZVP and RHF/TZVP models significantly overestimate the magnitude of EMS cross section at $\phi \leq 2^\circ$. Comparison of the B3LYP/TZVP and RHF/TZVP model calculations with the experimental results indicates that in the B3LYP model the electron correlation energy in the XC functional (V_{xc}) is too small in the long-range region for this orbital.

The orbital MDs of the 8a molecular orbital (peak 6), which are shown in figure 10, indicate quite large discrepancies between the different theoretical calculations and the experimental measurements. This is particularly evident in the low momentum region which is very sensitive to the electron XC energies of the molecule. Here we note that the BP/TZVP model MD is in good agreement with the EMS data over the azimuthal angular range $\phi < 8^\circ$, suggesting that the V_{xc} functional in the BP DFT functional is adequate for this orbital of BCHD in the long-range r-region. Note, however, that the BP/TZVP model does underestimate the magnitude of the orbital MD in the region $\phi = 10\text{--}20^\circ$. On the other hand, the RHF/TZVP and B3LYP/TZVP models generate reasonable agreement in the range $6^\circ \leq \phi \leq 10^\circ$, but fail a little thereafter. The overall discrepancies between the calculated and measured orbital MDs, with no theoretical calculation generating reasonable agreement over the entire angular range, indicate that the V_{xc} energy behaves inappropriately in this MO, and also that the electron V_{xc} energy is symmetry, orbital and momentum dependent. Moreover, the failure of the RHF/TZVP model in the low momentum region, suggests that the 8a MO involves a large degree of electron correlation energy.

The last orbital MDs to be considered correspond to peak 9 in the binding energy spectra and represent the combined 7a, 5b and 6a molecular orbitals. These are shown in figure 11.

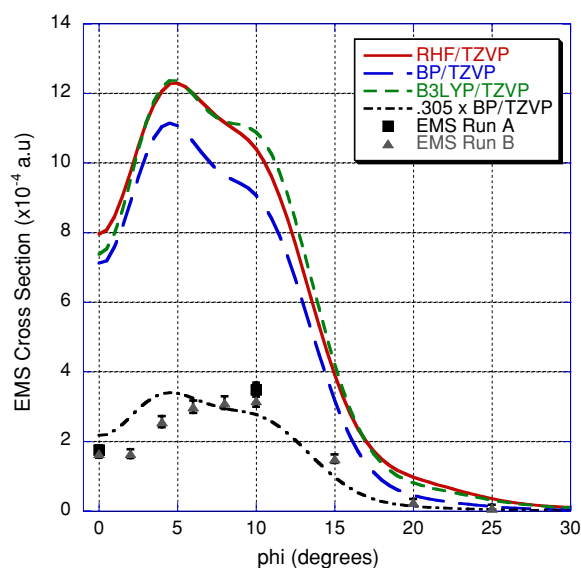


Figure 11. The 1500 eV symmetric non-coplanar momentum density for the 7a + 5b + 6a orbitals of BCHD ($\epsilon_f = 16.6$ eV). The EMS experimental measurements for run A (■) and run B (▲) are compared against PWIA calculations using RHF (—), BP (---) and B3LYP (- - -) model chemistries. Also shown is the the BP/TZVP model chemistry result scaled by a factor of 0.305 (- · - ·).

Here we note the significant variation observed between the theoretical and experimental magnitudes. This phenomenon could indicate a break down of the one electron picture of ionization, although a Green's function calculation at least to the third-order algebraic diagrammatic construction (ADC(3)) level would be needed to clarify this. Nonetheless if there was a splitting of one or more of these orbitals into two or more poles, the large discrepancy, at least in part, between the magnitude of theory and experiment for this summed MD might be explicable in their being some 7a, 6a or 5b flux lying outside the present experimental binding energy range. In figure 11 we have assigned a 'spectroscopic strength' of ~ 0.3 (as determined through a least-squares normalization technique) to the combined 7a + 6a + 5b orbital MD. The BP/TZVP model has then been scaled accordingly and is shown as a representative example in our figure 11. Here we note that the shape of the MD is in generally fair accord with the experimental data, although there are still differences in some details and we note that this variation is consistent across all theoretical models.

Further sources for these discrepancies might be due to a breakdown in our plane wave impulse approximation description for the reaction mechanism, although we are still dealing with outer valence states in this case so that we would not expect such an effect to explain away all the observed discrepancies. Rather it is more likely that none of the current model chemistries for one or more of the 7a, 6a and 5b MOs, is accurately producing a physical description for them. Indeed it is possible that all three of the explanations, for the significant differences in magnitude between theory and experiment, that we have proffered are making a contribution here.

Certainly, within the PWIA framework, it would be interesting to calculate MDs directly from relevant Dyson orbitals, such as those associated with the ADC(3) calculations from the Hasselt group [11, 35]. This would require an interface to be developed between the Flinders and Hasselt codes, a desirable development which is currently not available.

The orbital MDs were also measured and calculated for the outer valence 10a + 10b, 9b, 8b + 7b and 6b molecular orbitals. These data may be discussed further elsewhere, but only if they provide any further insight into the chemical bonding mechanism of this species.

5. Conclusions

We have reported on a comprehensive study of HREMS and PES measurements and DFT, HF and outer valence Green's function theory calculations into the outer valence electronic structure of bicyclo[2.2.1]hepta-2,5-dione. The results of this study significantly expand our knowledge of the electronic structure of this bicyclic species. In general good agreement was found between our EMS and PES experimental binding energies, and the binding energies theoretically obtained using accurate SAOP and OVGf calculations. In addition, where we were reasonably able to derive them, our EMS spectroscopic factors were found to be largely consistent with those predicted by our OVGf results. The orbital based momentum distributions of the outer valence shell for bicyclo[2.2.1]hepta-2,5-dione demonstrated that the electron exchange-correlation potential, V_{xc} , was dependent on the molecular symmetry, the orbital and the momentum region. With particular respect to the experimental orbital MDs and theoretically simulated orbital MDs using the RHF/TZVP model, we were able to comment on the accuracy of the V_{xc} functionals of our various DFT models on an orbital by orbital basis, thereby possibly contributing to the improvement, development and validation of density functional theory and the development of new density functionals. The present study showed that while not being nearly as impressive as that found in the case of stella-2,6-dione [3], indicating that the lower symmetry of BCHD compared to that of stelladione further complicates the chemical bonding and the role of the V_{xc} functional, the BP/TZVP model provided an overall fair quantitative representation of the exchange-correlation energy, on an orbital by orbital comparison basis, for the outer valence shell of bicyclo[2.2.1]hepta-2,5-dione. This description was clearly not perfect (and in some cases it was in fact quite poor), but it remained the best from the model chemistries considered. Finally, the present work clearly demonstrates that the quality of a theoretical model must be assessed using both the energy and wavefunctions in this regard.

Acknowledgments

This work is partly supported by the Australian Research Council. DBJ acknowledges financial support from the Ferry Trust and the Division of Complex Systems Science of the CSIRO. SS and FW acknowledge Professor D P Chong for useful discussions on accurate DFT binding energy calculations and the Australian Partnership for Advanced Computing (APAC) for use of the National Supercomputing Facilities. RG acknowledges support from the Deutsche Forschungsgemeinschaft, while MAB is indebted to the Shahid Bahonar University of Kerman and Flinders University for their support that enabled him to be a part of this work.

References

- [1] McCoy E F and Sykes M J 2003 *J. Chem. Inf. Comput. Sci.* **43** 545
- [2] Weigold E and McCarthy I E 1999 *Electron Momentum Spectroscopy* (New York: Kluwer)
- [3] Nixon K L, Wang F, Campbell L, Maddern T, Winkler D A, Gleiter R, Loeb P, Weigold E and Brunger M J 2003 *J. Phys. B: At. Mol. Opt. Phys.* **36** 3155
- [4] Altmayer M, Gaa B, Gleiter R, Rominger F, Kurzawa J and Schneider S 2001 *Eur. J. Org. Chem.* **2001** 3045
- [5] Brunger M J and Adcock W 2002 *J. Chem. Soc. Perkin Trans.* **2** 1

- [6] Hawkins R T, Hsu R S and Wood S G 1978 *J. Org. Chem.* **43** 4648
- [7] Mackenzie-Ross H, Brunger M J, Wang F, Adcock W, Trout N, McCarthy I E and Winkler D A 2002 *J. Electron Spectrosc. Relat. Phenom.* **123** 389
- [8] Mackenzie-Ross H *et al* 2002 *J. Phys. Chem. A* **106** 9573
- [9] Deleuze M, Pickup B T and Delhalle J 1994 *Mol. Phys.* **83** 655
- [10] Szabo A and Ostlund N S 1989 *Modern Quantum Chemistry: Introduction to Advanced Electronic Structure Theory* (New York: McGraw-Hill)
- [11] Knippenberg S, Nixon K L, Mackenzie-Ross H, Brunger M J, Wang F, Deleuze M, Francois J -P and Winkler D A 2005 *J. Phys. Chem. A* **109** 9324
- [12] Nooijen M and Snijders J G 1995 *J. Chem. Phys.* **102** 1681
- [13] McCarthy I E and Weigold E 1991 *Rep. Prog. Phys.* **54** 789
- [14] Becke A D 1988 *Phys. Rev. A* **38** 3098
- [15] Becke A D 1988 *J. Chem. Phys.* **88** 2547
- [16] Perdew J P 1986 *Phys. Rev. B* **33** 8822
- [17] Becke A D 1993 *J. Chem. Phys.* **98** 5648
- [18] Lee C, Yang W and Parr R G 1988 *Phys. Rev. B* **37** 785
- [19] Godbout N, Salahub D R, Andzelm J and Wimmer E 1992 *Can. J. Chem.* **70** 560
- [20] Andzelm J and Wimmer E 1992 *J. Chem. Phys.* **96** 1280
- [21] Komornicki A and Fitzgerald G 1993 *J. Chem. Phys.* **98** 1398
- [22] Schmidt M W *et al* 1993 *J. Comput. Chem.* **14** 1347
- [23] Frisch M J *et al* 2004 *Gaussian 03* Revision C.02 (Wallingford, CT: Gaussian)
- [24] Dunning T H Jr 1989 *J. Chem. Phys.* **90** 1007
- [25] Koopmans T 1933 *Phys. (Amsterdam)* **1** 104
- [26] Buijse M A, Baerends E J and Snijders J G 1989 *Phys. Rev. A* **40** 4190
- [27] Gritsenko O V, van Leeuwen R and Baerends E J 1994 *J. Chem. Phys.* **101** 8955
- [28] Chong D P, Gritsenko O V and Baerends E J 2002 *J. Chem. Phys.* **116** 1760
- [29] Takahata Y, Chong D P and Segala M 2004 *J. Braz. Chem. Soc.* **15** 282
- [30] Gritsenko O V, van Leeuwen R and Baerends E J 1995 *Phys. Rev. A* **52** 1870
- [31] Gritsenko O V, Schipper P R T and Baerends E J 1999 *Chem. Phys. Lett.* **302** 199
- [32] Baerends E J *et al* 2002 ADF version 03, <http://www.scm.com>
- [33] Chong D P, van Lenthe E, van Gisbergen S and Baerends E J 2004 *J. Comput. Chem.* **25** 1030
- [34] Cederbaum L S and Domcke W 1977 *Adv. Chem. Phys.* **36** 205
- [35] Knippenberg S *et al* 2004 *J. Chem. Phys.* **121** 10525
- [36] Wang F, Brunger M J and Winkler D A 2004 *J. Phys. Chem. Solids* **65** 2041
- [37] Ning C G, Ren X G, Deng J K, G L Su, Zhang S F and Li Q G 2006 *Phys. Rev. A* **73** 022704
- [38] Frost D C, Westwood N P C and Werstiuk N H 1980 *Can. J. Chem.* **58** 1659